INNER STRUCTURE OF CLOUD CAVITY ON A FOIL SECTION

Y. Kawanami[*]
National Maritime Research Institute[†]
Tokyo Japan

H. Kato
Toyo University
Saitama Japan

H. Yamaguchi, M. Maeda, S. Nakasumi
The University of Tokyo
Tokyo Japan

Abstract

Collapsing stage of cloud cavity and resulting violent shock pressure have been investigated by many researchers, because the knowledge of cavitation erosion is of practical importance and the dynamics is one of the most challenging problems in the field of two-phase flow. When a researcher intends to investigate the phenomenon numerically or experimentally, he or she must know the structure of the cloud cavity. The authors investigate cloud cavity, employing an off-axis laser holography system. This paper is a brief report concerning the inner structure of cloud cavity on a foil section.

1 Introduction

The dynamics of cloud cavitation and its erosive effect have been investigated through experiment or numerical simulation (Mϕrch (1981), Kubota et al (1989), d'Agostino & Brennen (1989), Le et al (1993), Kumar & Brennen (1993), Matsumoto & Shimada (1997), Stuz & Reboud (1997), Kawanami et al (1998)).

However the inner structure of cloud cavity is not yet sufficiently uncovered. This is the motivation of the authors to investigate the inner strucre of cloud cavity.

2 Experimental apparatus

The experiments ware made using Marine Propeller Cavitation Tunnel at The University of Tokyo. The authors used the foil test section of the tunnel. A two dimensional hydrofoil whose cross section was NACA0015 was selected as a test body. The hydrofoil was sustained by two struts which were fixed at the bottom of the test section. The chord length of the foil was 0.08 m and the aspect ratio was 1.875. The angle of incidence was 8.36 degree.

To investigate the inner structure of cloud cavity, the authors employed a laser holography system, which has been developed at The University of Tokyo (Yamaguch et al (1989), Maeda et al (1991), Kato et al (1999)). The optical system is composed of a ruby laser tube, an exciter, a set of mirrors and lenses, and hologram plate. The component was arranged on two optical benches. Figure 1 depicts the configuration of the optical system and optical pass of the laser beam. The axis of object beams was not identical that of reference beam (off-axis technique). The reference beam passed under the test section, whereas the object beam passed the suction side of the foil. The laser was a giant pulse ruby laser (NEO ARK Corp., type NGP-60MPE). The wavelength of the laser beam was 0.6943μm and the pulse width was 30 - 50 ns where the nominal output power was 300 - 500 mJ.

The diameter of object beam was expanded to 10mm or 30mm depending on the size of cloud cavity. It should be noted that the spatial resolution of hologram image becomes poorer as the expansion rate of the diameter of the object beam becomes larger. Table 1 shows the position of the object beam in terms of chord position on foil section.

[*] Domestic Research Fellow at Japan Science & Technology Corp.
[†] former Ship Research Institute

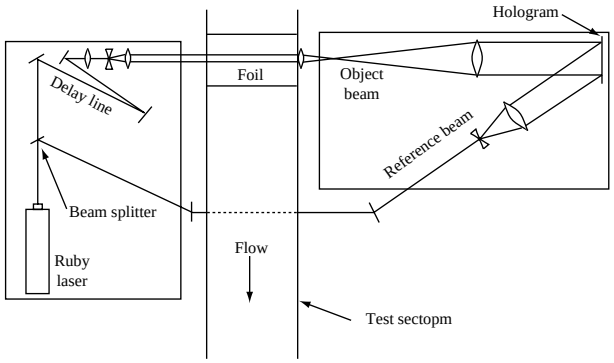

Figure 1: Laser holography system; top view

Table 1: Cavitation number and measurement chord position

σ	L_{CAV}/C	$37\%C$	$52\%C$	$58.6\%C$	$65\%C$
2.19	0.20	–	–	◯	–
1.86	0.25	◯	◯	–	◯
1.72	0.30	◯	◯	–	◯
1.61	0.40	–	◯	◯	◯

It was impossible to take the holographic image of the cloud cavity immediately after break-off because the void fraction of such cloud cavity was too high for the object beam be sufficiently diffracted in the cloud cavity and reach the hologram plate. So, our target was the cloud cavities which became relatively sparse after its break-off.

The authors reconstructed the holographic image of cloud cavity using a He-Ne gas laser. Radiating He-Ne laser beam to the hologram at the same angle of incidence as the reference beam, we could reconstruct twin images separately and analyze real image. The reconstructed real image was analyzed through a CCD camera. The images were scanned in the direction of foil span and analyzed on a PC.

In addition to the hologram, we mounted a camera on the top of the test section to shoot the cavitation appearance from the suction side of the foil at the same time of the ruby-laser pulsing. The still photographs taken by the camera were used to determine which cavity was analyzed in the holographic image (for example see Figure 5 (b)). The details of the holography system are described by Maeda et al (1991).

3 Experimental conditions

The angle of incidence was fixed at 8.36 degree and uniform flow velocity was 8.0 m/s resulting in the Reynolds number $Re = 5.0 \times 10^5$. The cavitation number was ranged from 2.19 to 1.61 where sheet cavity length L_{CAV} was $20 - 40\%C$ approximately as shown in Table1.The air content of circulating water was 5 - 10% of that of saturated water under atmospheric pressure.

4 Appearance of cloud cavity and analysis method

To obtain holographic image of a cloud cavity, the authors needed to know the size of the cloud cavity passing through the object beam beforehand. So we made a preliminary experiments. We took a broad survey on the maximum length of sheet cavity (L_{CAV}) and how the size of cloud cavity changed with cavitation number. When cavitation number was low, the sheet cavity blocked off the laser beam and the size of the cloud cavity was larger than the scope of the expanded object beam, both resulting in poor holographic image. With large cavitation number, on the other hand, the cloud cavity became too small to analyze the inner structure of the cavity with sufficient spatial resolution. Taking

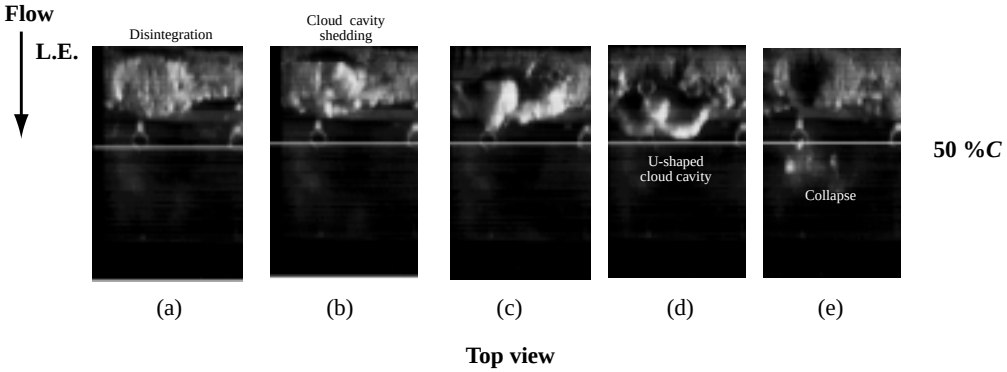

Figure 2: Time sequence of photographs of a cloud cavity based on the high-speed video image; $\sigma = 1.72$; $\alpha = 8.36\,°$; $U_\infty = 8.0$m/s

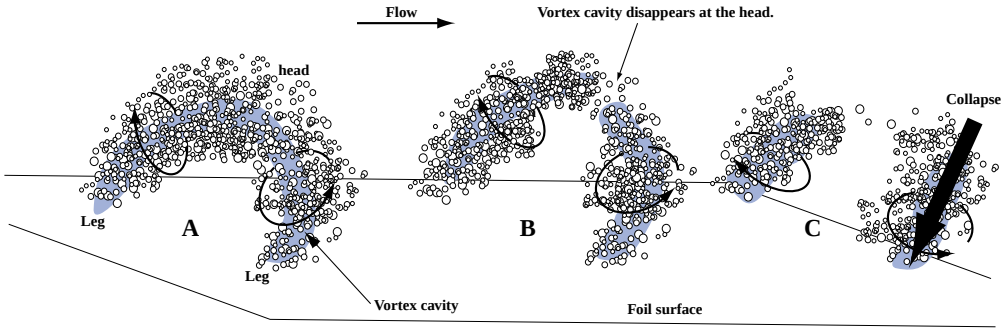

Figure 3: Transformation of a cloud cavity (schematic diagram)

these results of the preliminary experiment into account, cavitation number was set in the range of 1.61-2.19 where $20\%C \leq L_{CAV} \leq 40\%C$.

Figure 2 shows an example of the sequence of photographs based on the high-speed cine observation where the frame speed of the high-speed video camera is 4500 frame/sec. The sheet cavity grows to its maximum and is disintegrating into a bubble cluster (a). The bubble cluster is shed downstream as a cloud cavity (b). The cloud cavity is distorted into U-shaped vapor structure as it moves downstream apart from new sheet cavity (c,d) and finally violent collapse occurs (e). In this case, we could obtain good hologram image of the cloud cavity which was at the stage (c) - (e), whereas the bubble cluster or the cloud cavity at the stage (a) and (b) could not captured by the object beam due to the size or the high void fraction of the cavity.

Figure 3 depicts the three stages of a typical cloud cavity from break-off to violent collapse based on the observation through naked eye, high-speed video camera and still photographs. The cloud cavity at stage A corresponds to that of stage (d) in Figure 2. At this stage, the cloud cavity consists of one vortex cavity (vortex core) and many cavity bubbles surrounding it. The vortex cavity and cavity bubbles form U-shaped vapor structure as a whole (one head and two legs). Circulation around cloud cavity is clearly observed. One possible explanation of the source of the circulation is re-entrant jet (Le et al (1993), Kawanami et al (1996)). However the discussion should be deepened based on the further investigations.

While moving downstream, the U-shaped cloud cavity split up into two or more vapor structures (stage B). In most cases, the split occurs at the head of the U-shaped cloud cavity. Then, the individual vapor structure collapses toward foil surface along its axis in high pressure region (stage C or stage (e) in Figure 2). Erosion pits on the foil surface concentrated in the area where cloud cavity at stage C was observed.

Analysis of hologram image was made as follows:

- A reconstructed image was displayed on a CRT monitor through CCD camera which was mounted on a traverser and capable of traversing in the direction of foil span. In a cross section at one end of the targeted cloud cavity, the position, the radius and the number of cavity bubbles were measured. Approximate shape of the vortex cavity was also measured.

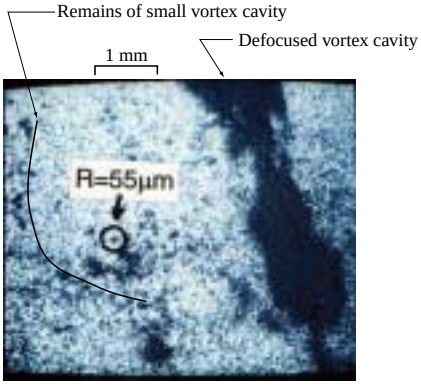

Figure 4: Reconstructed image of cloud cavity; Focused bubble and defocused vortex cavity

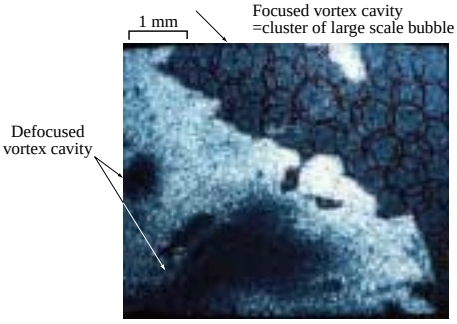

Figure 5: Reconstructed image of cloud cavity; Focused and defocused vortex cavity

- The CCD camera was traversed in the direction of foil span proceeding to next cross section.
- The above two procedure are repeated until the another end of cloud cavity was reached.

In Figure 2, the cloud cavity appears to be composed of a vortex cavity surrounded by small bubble cavities. The situation can be confirmed in greater detail on the reconstructed holographic images. Figures 4 and 5 show examples of the cross sections of the reconstructed images. These image are enlarged by the CCD camera to measure the size of cavity bubble. In the analysis procedure, the image was enlarged by nine times larger than the image in Figures 4 and 5 to measure bubble radius with sufficient accuracy.

In Figure 4, focused cavity bubble (55μm radius) is indecated and defocused vortex cavity are observed. The holography system employed in the present measurement had sufficient spatial resolution to measure a cavity bubble of 5 μm radius. However, it is not practical and terribly time consuming to measure or count small bubbles which don't have significant effects from the cavitation erosion point of view. So, the authors took account of moderately large bubbles. The minimum radius of bubble counted was determined 10 μm and 35 μm corresponding to the object beam diameter of 10 mm and 30 mm respectively. This threshold values were sufficiently small compared to the diameter of typical erosion pits, that is, several hundred μm approximately.

There is a chain of cavity bubbles next to the 55μm-radius bubble, which is a remain of thin vortex cavity. The chain of cavity bubbles or thin vortex cavity was offten observed around main vortex cavity which forms cloud cavity. One of the authors thinks that the thin vortex cavity is due to the free shear layer (vortex sheet) on the surface of the sheet cavity which is the source of cloud cavity, whereas the main vortex cavity is formed by re-entrant jet. The boundary layer flow on sheet cavity surface was investigated by Arakeri et al (1969), Brennen (1970) and Franc & Michel (1985). In Figure 5, on the other hand, focused and defocused vortex cavities are observed. A vortex cavity in the hologram image could be recognized as focused or defocused one dependig on the position of the CCD camera.

It was, however, very difficult to measure the volume or shape of the vortex cavity accurately. So the authors measured the approximate position of the focused vortex cavity in each measuring section assuming that the vortex cavity was a cluster of virtual large scale bubbles. The many circles on the focused vortex cavity (Figure 5) represent such virtual large bubbles.

5 Reconstructed images of cloud cavity

Figure 6 (a) is a reconstructed image of a cloud cavity, where $\sigma = 1.86$, $L_{CAV} = 25\%C$, and the center of the expanded object beam was at 52 %C. Figure 6 (b) is a still photograph taken at the same time as the reconstructed image. The cloud cavity enclosed by white rectangular frame corresponds to the one in Figure 6 (a). As seen in Figure 2 (d), it was confirmed that cloud cavity formed U-shaped vapor structure at this condition indecated by yellow dashed line in Figure 6 (a). Although the U-shaped cloud cavity is observed, one leg of the cloud cavity is already collapsed into cavity bubbles. Small chains of cavity bubbles are observed near the head of U-shaped structure and around the vortex cavity as indicated by black solid lines. These chains of cavity bubbles are remains of thin vortex cavities. The main vortex cavity was already collapsed in the head. The cloud cavity in the reconstructed image is classified the one at the stage C in Figure 3. From the observation through the high-speed video camera, the cloud cavity immediately after this stage collapses toward the foil surface along the axis of its leg. The angle between the leg and the foil surface is 40 degree approximately. Similar U-shaped structure was observed by Joussellin et al (1991). Investigating relatively short sheet cavitation, they referred the U-shaped vapor structure as horseshoe vortex cavity This indicates that cloud cavity on foil section is a kind of vortex cavity which accompanies many cavity bubbles around it.

(a) Reconstructed image (side view)

(b) Still photograph (top view)

Figure 6: Reconstructed image and still photograph of a cloud cavity

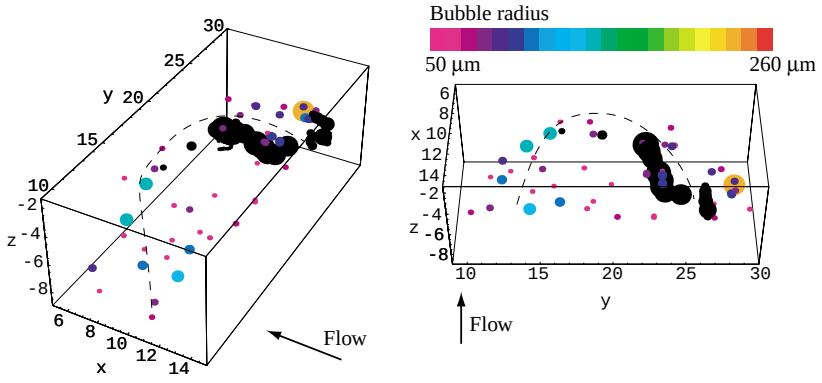

(a) Bird's eye view

(b) Front angular view

Figure 7: Bubble distribution in a cloud cavity at 52%C; $\sigma = 1.86$; $\alpha = 8.36$ °; $U_\infty = 8.0$m/s

Figure 7 is the result of analysis on the hologram image Figure 6 (a) and shows simplified bubble distribution in the cloud cavity. Small bubbles, less than 50μm in radius, are omitted from the figure to avoid unnecessary complication. Blobs of overlapping black sphere represent vortex cavity,while other spheres are cavity bubbles. It is clear that the vortex cavity and relatively large bubbles form the U-shaped vapor structure as a whole as indicated by black dashed line.

Figure 8 is another example of reconstructed image, where $\sigma = 1.61$, $L_{CAV} = 40\%C$, and the center of the expanded object beam was at 65 %C. In this case, the U-shaped vapor structure is clearly obserbed, espesialy the two legs are thik. The votex cavity split up into major four parts, that is, the two legs and two remains of the head. These parts form the U-shaped vapor structure (yellow dashed line). There are small chains of cavity bubbles around the head (Figure 8 (b)). The standing angle is about 75 degree.

Figure 9 contains two reconstructed images, where $\sigma = 1.61$, $L_{CAV} = 40\%C$ and the center of the object beam was $65\%C$. The cloud cavity was larger than that in Figure 6 and Figure 8. Again the U-shaped vapor structure is observed as indicated by yellow dashed line. In Figure 9 (a) one of the leg structure is focused, whereas in Figure 9 (b) the another leg is focused. The main vortex cavity splits up into several parts and some chains of cavity bubbles are observed around it. The main parts of the vortex cavity are apart from each other, nevertheless they form the U-shaped vapor structure. This indecates the existence of flow structure with strong circulation. The angle between leg #2 and foil surface is about 75 degree. Leg #1 does not touch the foil surface.

Figure 10 shows bubble distribution in the cloud cavity which presents in the reconstructed image, Figure 9. The U-shaped structure is more prominent than that of the previous cloud cavity.

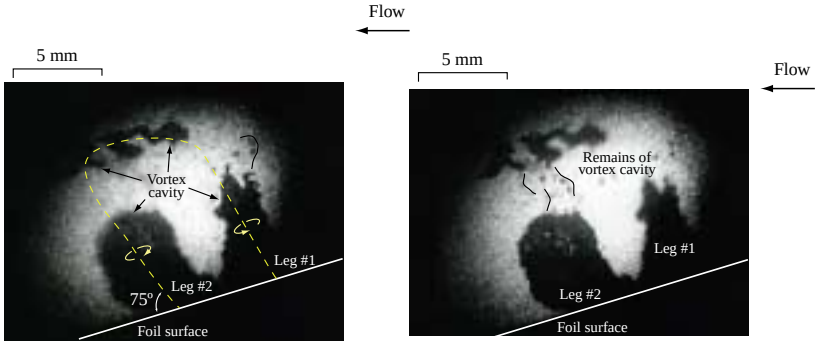

(a) Reconstructed image; Leg #1 is focused. (b) Reconstructed image; Leg#2 is focused.

Figure 8: Reconstructed images of cloud cavity; $\sigma = 1.61$; $\alpha = 8.36\,°$; $U_\infty = 8.0$m/s; Center of object beam = $65\%C$

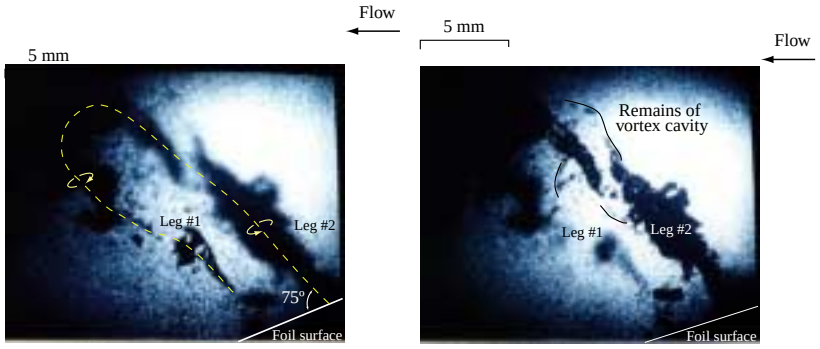

(a) Reconstructed image; Leg #1 is focused. (b) Reconstructed image; Leg#2 is focused.

Figure 9: Reconstructed images of cloud cavity; $\sigma = 1.61$; $\alpha = 8.36\,°$; $U_\infty = 8.0$m/s; Center of object beam = $65\%C$

6 Bubble distribution in cloud cavity

The authors analyzed ten hologram images. The number of bubbles, the position and the size of the individual bubble were counted or measured on each reconstructed image. The number of bubbles contained in a cloud cavity ranged from few thousands to a hundred thousand or above. As mentioned in the section 2, the small bubble whose radius was less than 10 or 35 μm was not counted.

Figure 11 shows the bubble number distributions in cloud cavity under various cavitation number and chord position on the foil. The ordinate is bubble number distribution (m^{-4}) and the abscissa is bubble radius R (m). In this figure, the results of Maeda et al (1991) and Yu & Ceccio (1996) are shown together with the present results. The authors made experiments with low-air-content water around 10% in terms of dissolved oxygen. It should be noted that the distributions are 'bubble' number distributions and the vortex cavities which is at the center of cloud cavity are not taken into account. Yu & Ceccio measured the bubble number distribution in the far wake behind relatively short sheet cavity with relatively higher-air content water.

The bubble number distributions are somewhat scattered. However, there is no prominent difference in the distributions in spite of different chord position of cloud cavity and different cavitation number. First, let us consider the reason why the distribution is not affected by the chord position of the cloud cavity. As mentioned in the previous section, vortex cavity exists in the center of cloud cavity and sustains the cloud cavity with the low pressure. As the cloud cavity moves to high pressure region, surrounding cavity bubbles shrink and are out of our scope, whereas the vortex cavity split up supplying new cavity bubbles in the cloud cavity. This shrinkage and supply make the distribution not change significantly due to the chord position of the cloud cavity.

Next, the effect of cavitation number on the distribution is important. The distribution was calculated based on the total number of bubbles divided by the measurement volume. When the cavitation number is small, the cloud cavity is large and the number of bubbles included in the cavity is large. At the same time, the measurement volume becomes large. That makes the distribution not be strongly affected by the cavitation number.

The present results can be approximated as

$$N = aR^k.$$

In the present case, the exponent k equals -5.1. It should be noted that the approximation holds relatively large

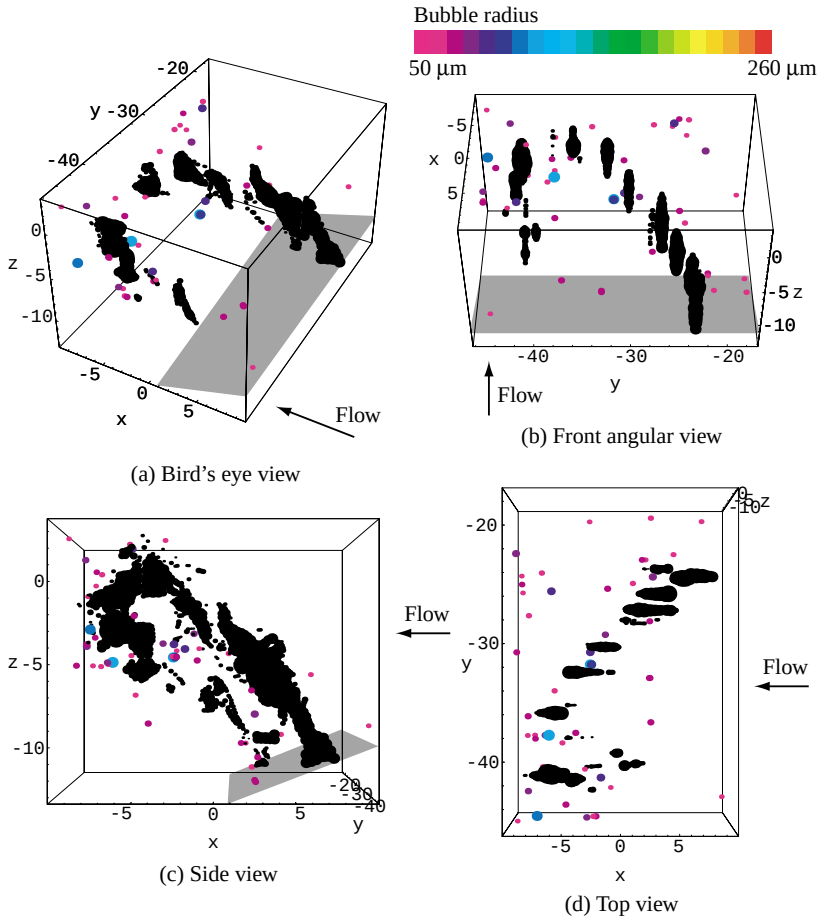

(a) Bird's eye view

(b) Front angular view

(c) Side view

(d) Top view

Figure 10: Bubble distribution in a cloud cavity at $65\%C$; $\sigma = 1.61$; $\alpha = 8.36$ °; $U_\infty = 8.0$m/s

bubbles ($R \geq 35\mu$m, in this case).

7 Concluding remarks

Using off-axis laser holography system, the authors investigated the inner structure of cloud cavity on a two-dimensional foil. Major findings are as follows:

1. The cloud cavity observed on hydrofoil is an U-shaped vapor structure with cavity bubbles surrounding it. The two ends of the vortex touch foil surface.
2. Violent collapse leading to erosive shock occurs along the legs of the U-shaped vapor structure.
3. The bubble number distribution (N) can be approximated as,

$$N = aR^k,$$

where $k = -5.1$ in the present case.

Acknowledgements

The authors appreciate the effort of Mr. Miyanaga at The University of Tokyo. They also thank the members of Propulsor Section at National Maritime Research Institute, Dr. Ukon, Dr.Kudo, Mr. Matsuda and Mr. Fujisawa, for their valuable discussions and supports through the preparation of this report.

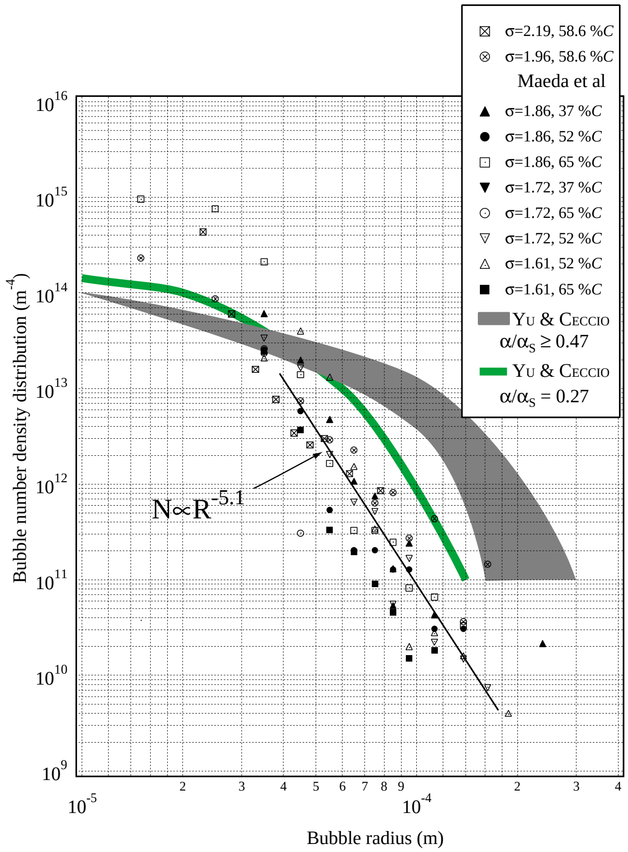

Figure 11: Bubble number distributions in cloud cavity at various cavitation number

References

Mϕrch, K. A. (1981) *Proc. ASME*,1-10.
Kubota, A., Kato, H., Yamaguchi, H. and Maeda, M. (1989) *ASME J. of Fluids Eng.*, **111**, 204-210.
d'Agostino, L. and Brennen, C. E. (1989) *J. of Fluid Mech.*, **199**, 155-176.
Kumar, S. and Brennen, C. E. (1993) *J. of Fluid Mech.*, **253**, 565-591.
Matsumoto, Y. and Shimada, M. (1997) *Proc. ASME FED*
Stutz, B. and Reboud, J. L. (1997) *Experiments in Fluids*, **22**, 191-198.
Yamaguchi,H., Kato, H., Maeda, M. and Kamijo, A. (1990) *Proc. ASME FED*, **98**, 115-119.
Maeda, M., Yamaguchi, H. and Kato, H. (1991) *Proc. ASME FED*, **116**, 67-75.
Kato, H., Yamaguchi, H. Maeda, M., Kawanami, Y. and Nakasumi, S. (1999) *J. of Visualization*, **2**, 37-50.
Arakeri *ASME J. of Fluids Eng.*, **115**, 243-248.
Brennen, C. E. (1970) *J. of Fluid Mech.*, **44**, 33-49.
Franc, J. P. and Michel, J. M. (1985) *J. of Fluid Mech.*, **154**, 63-90.
Le, Q., Franc, J. P. and Michel, J. M. (1993) *ASME J. of Fluids Eng.*, **115**, 243-248.
Kawanami, Y., Kato, H., Yamaguchi, H., Tagaya, Y. and Tanimura, M. (1997) *ASME J. of Fluids Eng.*, **119**, 788-794.
Joussellin, F., Delannoy, Y., Sauvage-Boutar, E. and Goirand, B. (1991). *Proc. ASME FED*, **116**, 61-66.